ELSEVIER

Matrix Biology 21 (2002) 139–147

MATRIX BIOLOGY

www.elsevier.com/locate/matbio

A structural model for force regulated integrin binding to fibronectin's RGD-synergy site

André Krammer[a,1], David Craig[a], Wendy E. Thomas[a], Klaus Schulten[b], Viola Vogel[a,*]

[a]*Department of Bioengineering, University of Washington, Seattle, WA 98195, USA*
[b]*Beckman Institute, University of Illinois at Urbana-Champaign, Urbana, IL 61801, USA*

Received 12 July 2001; received in revised form 15 November 2001; accepted 19 November 2001

Abstract

The synergy site on fibronectin's FN-III$_9$ module, located approximately 32 Å away from the RGD-loop on FN-III$_{10}$, greatly enhances integrin $\alpha_5\beta_1$ mediated cell binding. Since fibronectin is exposed to mechanical forces acting on the extracellular matrix in vivo, we used steered molecular dynamics to study how mechanical stretching of FN-III$_{9-10}$ affects the relative distance between these two synergistic sites. Our simulations predict the existence of an intermediate state prior to unfolding. In this state, the synergy–RGD distance is increased from 32 Å to approximately 55 Å, while the conformations of both sites remain unperturbed. This distance is too large for both sites to co-bind the same receptor, as indicated by experiments that confirm that increasing the length of the linker chain between FN-III$_9$ and FN-III$_{10}$ reduces $\alpha_5\beta_1$ binding. Our simulations thus suggest that increased $\alpha_5\beta_1$-binding attributed to the synergy site, along with the associated downstream cell-signaling events, can be turned off mechanically by stretching FN-III$_{9-10}$ into this intermediate state. The potential physiological implications are discussed.

Keywords: Steered molecular dynamics; Fibronectin; Synergy site; RGD loop; Mechanical force

1. Introduction

The extracellular matrix protein fibronectin (FN, shown in Fig. 1) contains a synergy site that selectively enhances binding of certain integrins to the neighboring RGD-loop by over forty-fold (Grant et al., 1997). Integrins that recognize the synergy site and RGD-loop of FN include $\alpha_5\beta_1$ and $\alpha_{IIb}\beta_3$. In contrast, integrins such as $\alpha_v\beta_3$ bind FN's RGD-loop, but are unaffected by the presence of the synergy site. One apparent function of this synergy site is to allow integrin $\alpha_5\beta_1$ to bind FN preferentially over other RGD-containing matrix proteins (Corbett and Schwarzbauer, 1999; Danen et al., 1995; Sechler et al., 1997). Recent studies have suggested that the increase in FN-$\alpha_5\beta_1$ binding is dependent on the relative spatial position between these two sites (Garcia et al., 1999; Grant et al., 1997). FN, with its synergy site, not only initiates downstream intracellular signaling events that are different from those induced by other RGD-containing matrix proteins (Wu et al., 1998), but only does so through different, yet to be defined, relative conformational states (Garcia et al., 1999). This observation raises the issue of why the synergy site and RGD-loop are located on separate, but neighboring modules, rather than together on a single module.

Steered molecular dynamics (SMD) simulations probe structural changes resulting from mechanical tension (Isralewitz et al., 2001a). Starting from high-resolution protein structures equilibrated in the presence of explicit water molecules, SMD simulates force-induced unfolding by applying force to the two termini of a protein module. Simulations are currently the only method to gain a highly detailed atomic level insight into how proteins change conformation in response to mechanical stretching. In contrast, experimental methods such as AFM and optical tweezers can probe forces and total extensions of stretched molecules, but cannot by themselves discern which bonds are broken or what inter-

* Corresponding author. Tel.: +1-2065431776; fax: +1-2066854434.
E-mail address: vvogel@u.washington.edu (V. Vogel).
[1] Current address: Accelrys Inc., 9685 Scranton Road, San Diego, CA 92121, USA.

0945-053X/02/$ - see front matter
PII: S0945-053X(01)00197-4

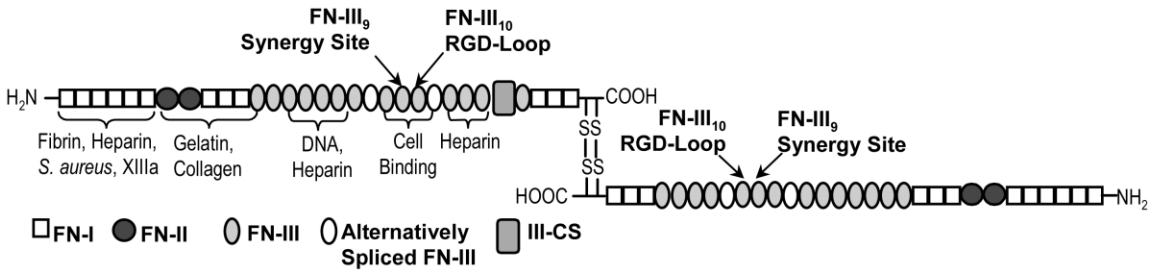

Fig. 1. Structure of the disulfide cross-linked fibronectin (FN) dimer and location of key binding sites. The synergy site and the RGD-loop are located on the ninth and 10th type III modules, FN-III_9 and FN-III_{10}, respectively.

mediate structures are involved (Kellermayer et al., 1997; Oberdorfer et al., 2000; Oberhauser et al., 1998; Rief et al., 1997). Moreover, the combined use of SMD simulations and AFM experiments on engineered mutants of titin modules have demonstrated that SMD can reliably predict the relative mechanical stability of homologous modules and the location of force bearing residues (Isralewitz et al., 2001b; Lu and Schulten, 1999, 2000; Marszalek et al., 1999).

In previous work, we have used SMD to explore the structural changes caused by mechanical force on individual type III modules of FN (FN-III). We have predicted: (1) that the RGD-loop is straightened once the G-strand breaks away, thereby eliminating high affinity binding to integrins (Krammer et al., 1999); (2) that FN-III_{10} is one of the mechanically weaker FN-III modules (Craig et al., 2001); and (3) that individual FN-III modules pass through a structural intermediate prior to the unraveling of the first β-strands under mechanical force (Craig et al., 2001). Since the β-strands of each β-sheet align themselves in parallel to the external force vector, this structural intermediate has been termed the 'aligned' state. In comparison, the β-sheets in the native FN-III modules exhibit a 'twisted' conformation. Here, we investigate how the interactions between the two modules of FN-III_{9-10} affects the early events of their forced unfolding pathway, as well as the relative distance and orientation of the synergy and RGD site. We provide a detailed structural analysis of the molecular events accompanying stretching and discuss the relevance of structural intermediates.

2. Methods

The FN-III_{9-10} structure was adopted from the X-ray crystallographic structure of the tetramer FN-III_{7-10} (PDB code: 1FNF) (Leahy et al., 1996). Molecular dynamics simulations were carried out in an explicit all-atom model with the CHARMM22 force field (MacKerell et al., 1998) and TIP3P (Jorgensen et al., 1983) water parameters using the program NAMD (Kale et al., 1999). FN-III_{9-10} was solvated by explicit water molecules in a periodic box measuring $260\times65\times65$ $Å^3$. All simulations were performed with a time step of 1 fs, a uniform dielectric constant of 1, and a cut-off for non-bonded forces with a switching function starting at a distance of 10 Å and reaching zero at 13 Å. The energy of the entire system was minimized in 200 steps. Thermalization was achieved by heating the system up to 300 K, in increments of 30 K for time intervals of 1 ps, while leaving the box volume unchanged. During equilibration, the simulation box was allowed to relax its size. This was accomplished by anisotropically coupling the system to a Berendsen pressure piston with a relaxation time of 0.5 ps and a compressibility factor of 4.46×10^{-5} bar^{-1}. The reference pressure of the system was set to 1 bar. After equilibrating the system for 50 ps, the simulation box measured $156\times64\times64$ $Å^3$ in dimension, resulting in an atom density of 0.100 $Å^{-3}$, and a stable solvated structure of FN-III_{9-10} that possesses a RMSD of 2.7 Å with respect to its crystal structure. During thermalization and equilibration, while the system was coupled to a Langevin heat bath, the protein terminal α-carbon atoms (C_αs) were held fixed to prevent drifting of the protein. The entire system contained 100 679 atoms, taking approximately one week of computational time on 64 SGI R10000 processors per nanosecond of simulation time.

All distances between residues are measured in regards to their C_αs unless otherwise noted. The tilt angle, defined as the angle between N-terminal C_α (Gly^1), the middle linker C_α (Val^{91}), and the C-terminal C_α (Thr^{184}), increases from 140° to approximately 175°. The rotation angle was defined as the dihedral angle formed by C_α of Arg^{54}, the center of masses for FN-III_9 and FN-III_{10}, and C_α of Arg^{168}.

Forced unfolding was accomplished through a constant force (cf-SMD) or a constant velocity (cv-SMD) protocol. In both cases, the N-terminal C_α atom (Gly^1) was constrained to a fixed position, while force was applied to the C-terminal C_α atom (Thr^{184}). Unfolding was accomplished in cf-SMD by applying a constant force to Thr^{184} along the direction of the vector connecting the two termini, the so-called extension vector (Lu and Schulten, 1999). Conversely, in cv-SMD the applied force was derived from a harmonic spring that

acts on Thr[184] and is moved with constant velocity in the direction of the extension vector. The pulling velocity was set to 0.5 Å/ps with a harmonic force constant of 10 $k_BT/Å^2$. The force used in cf-SMD simulations measured 750 pN.

3. Results

Fig. 2a shows a time–extension curve of a typical simulation in which FN-III_{9-10} is pulled with a constant force of 750 pN. Also shown are the corresponding extensions for the individual modules FN-III_9 and FN-III_{10} measured between C_αs of Gly[1] and Thr[90] and of Val[91] and Thr[184], respectively. While the time–extension curves of single FN-III modules in our previous studies displayed two distinct plateaus correlating to aligned and twisted states, the time–extension curve of FN-III_{9-10} here reveals a single plateau followed by a gradual increase of the extension interrupted by occasional shoulders. This is followed by a rapid increase in overall extension, beginning at an extension of 53 Å and a time of approximately 600 ps. An analysis of the differential contributions of the two modules to the total FN-III_{9-10} extension reveals that FN-III_9 remains trapped in the first plateau as time progresses, while FN-III_{10} undergoes further structural changes that finally lead to the unraveling of its tertiary structure.

We have also previously found that two main energy barriers must be overcome before the first β-strand breaks away in single FN-III modules. The crossing of the first energy barrier correlated with the breakage of two conserved backbone hydrogen bonds between the β-strands A and B that are located immediately following the β-bulge of the A-strand. Analysis of the FN-III_{9-10} trajectory reveals that the same two hydrogen bonds, between Arg[96] and Asp[113] on FN-III_{10}, break at the end of the first plateau as indicated by the black dashed line in Fig. 2. Breakage of these two hydrogen bonds precedes the alignment of the β-strands of $FNIII_{10}$ with respect to the external force vector (aligned state). The crossing of the second barrier corresponded to the rupture of a backbone hydrogen bond cluster and separation of the first β-strand. The breakage of the cluster of hydrogen bonds between F- and G-strands in FN-III_{9-10} is indicated by the gray dotted line in Fig. 2. Consistent with earlier simulations, rapid extension of FN-III_{9-10} was observed following the breakage of these hydrogen bonds. Characteristic stages in the forced unfolding pathway, as shown in Figs. 2 and 3, include as discussed later: (1) the equilibrated structure; (2) the pre-stretched state; (3) the functionally decoupled state; and (4) the subsequent unraveling of the FN-III modules. While all of the figures given below are from the same simulation, the sequence of events described here and the extensions at which they occur were essentially the same in a second cf-SMD (constant force pulling) and in two cv-SMD simulations (constant pulling velocity).

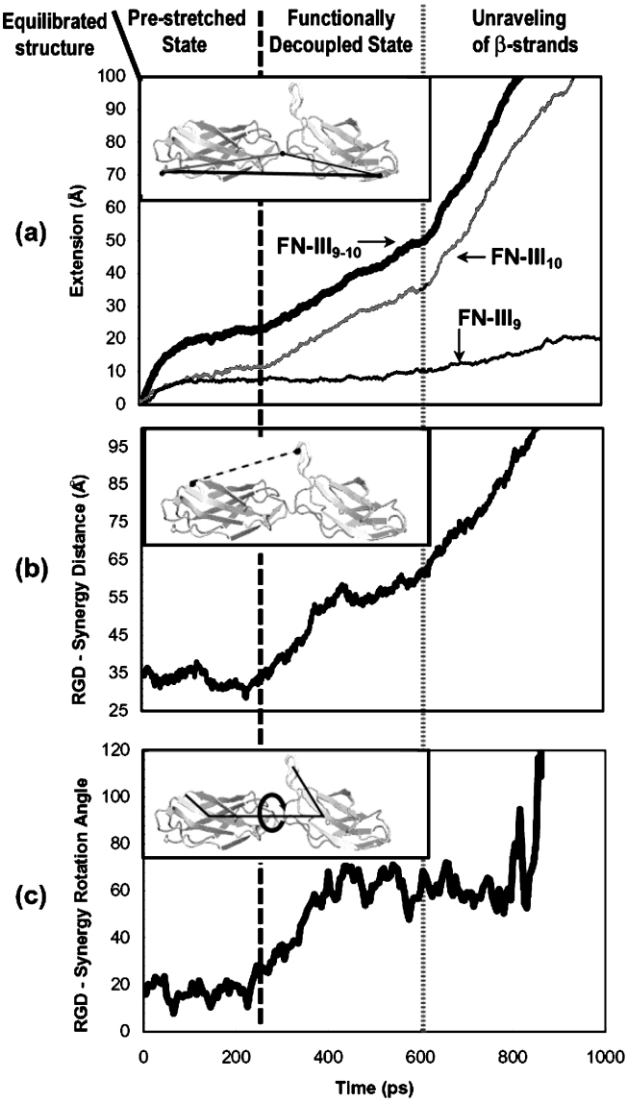

Fig. 2. (a) SMD derived extension-time profile for FN-III_{9-10} from cf-SMD simulation with an external applied force of 750 pN. Separate traces are given for the individual extensions of FN-III_9 and FN-III_{10} for the same simulation, defined as the distance between C_αs of Gly[1] and Thr[90] for FN-III_9 and C_αs of Val[91] and Thr[184] for FN-III_{10}. (b) The corresponding RGD-loop to synergy site distance (defined as the distance between C_αs Arg[54] and Arg[168]) and (c) relative rotational orientation (defined as the dihedral angle formed by the C_α of Arg[54], the center of masses for FN-III_9 and FN-III_{10}, and the C_α of Arg[168]) display two distinct plateaus. The black dashed line indicates the rupture of the backbone hydrogen bonds between Arg[96] and Asp[113] in FN-III_{10}. The gray dotted line indicates rupture of the first cluster of hydrogen bonds between the F- and G-strands of FN-III_{10}.

3.1. Equilibrated structure

The equilibrated structure refers to FN-III_{9-10} after equilibration in the presence of excess water without tension. Other than minor fluctuations found in the loop

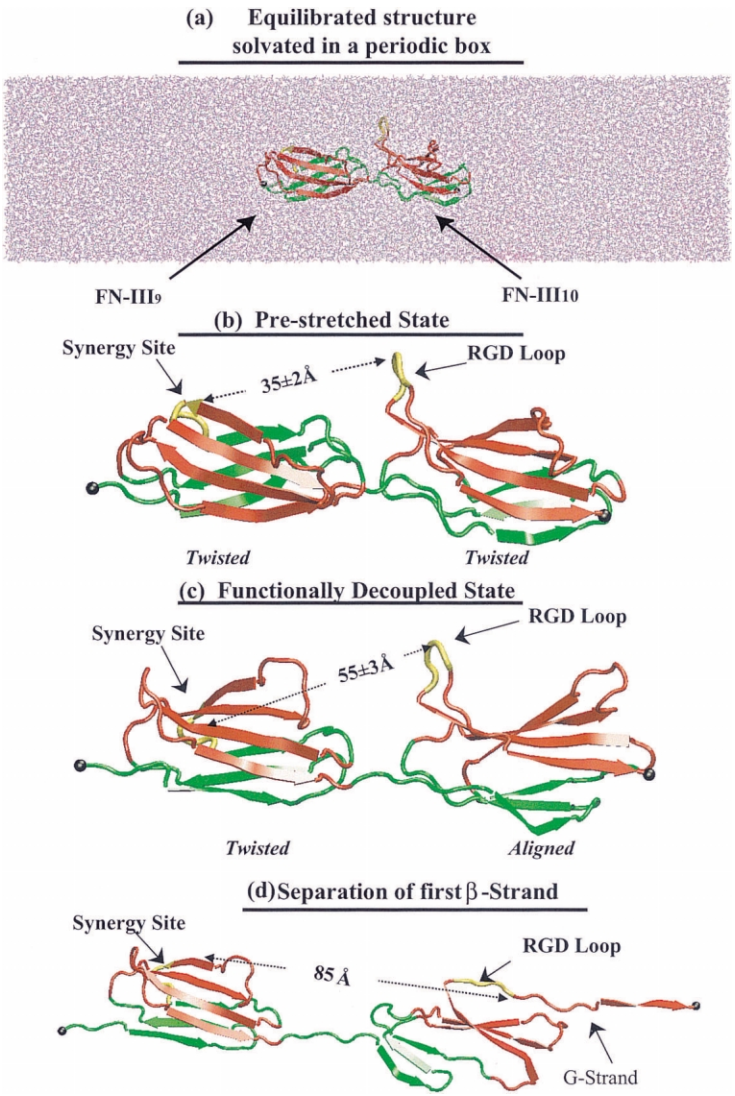

Fig. 3. Cartoon representation of (a) the initial equilibrated structure solvated in a periodic box with explicit water; (b) the pre-stretched state; (c) the functionally decoupled state; and (d) the separation of the first β-strand. Snapshots are taken at times 0, 200, 400 and 800 ps in the cf-750 pN simulation corresponding to extensions of 0, 20, 34 and 100 Å, respectively. For simplicity, the water box is only shown in (a). Modules are color-coded such that the upper β-sheets are red, the lower β-sheets are green and the RGD and synergy binding sites are in yellow. In the native and pre-stretched states, the time-averaged distance between the synergy site and RGD-loop is 35 ± 2 Å, while in the functionally decoupled state the time-averaged distance is 55 ± 3 Å. In later stages of this simulation the G-strand of FN-III$_{10}$ separates first, thereby straightening the RGD-loop. Frame (d) in the figure provides a snapshot of the subsequent unraveling process taken at a synergy–RGD distance of 85 Å.

and end-termini lacking secondary structure, the equilibrated structure (Fig. 3a) agrees closely with the crystal structure (Leahy et al., 1996), showing an C_α RMSD of only 2.7 Å.

3.2. Pre-stretched state

The ensemble of states found within the first plateau region of FN-III$_{9-10,}$ at an extension of 20 Å relative to the end-to-end distance of its equilibrated structure, is defined as the 'pre-stretched' state. Under a constant force of 750 pN, the pre-stretched state was reached in less than 50 ps (Fig. 2a). In addition, there were no significant force peaks prior to this state in our cv-SMD simulations (not shown). These results suggest that the pre-stretched state is reached by undergoing an elastic and reversible extension of FN-III$_{9-10}$. FN-III$_{9-10}$ is trapped in this state for an extended time period since a major energy barrier has to be overcome prior to further unfolding.

This initial extension occurs without significant loss of the secondary structure. The peptide linker sequence between FN-III$_{9-10}$ (Thr^{90}–Pro^{95}) stretches by approximately 7 Å. In addition, the FN-III$_{9-10}$ terminal ends (Gly^{1}–Pro^{5} and Tyr^{182}–Thr^{184}) straighten along the direction of the applied force vector and together yield

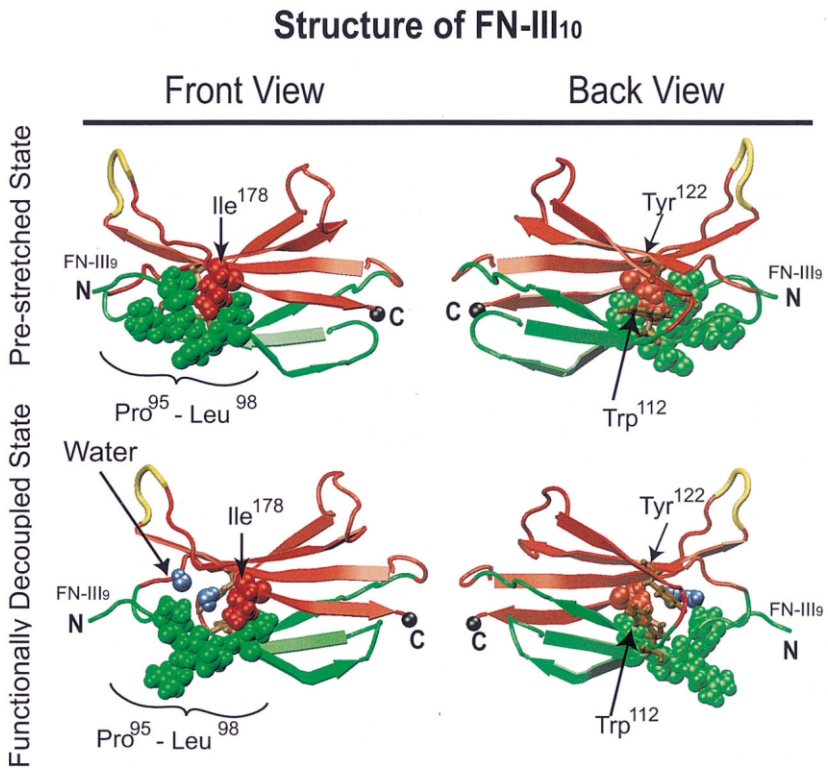

Fig. 4. Structural changes that accompany transition from the pre-stretched state to the functionally decoupled state for FN-III$_{10}$ (FN-III$_9$ is not shown for clarity). These changes include straightening of a β-bulge on the A-strand (residues shown as green spheres). Ile^{178} from the G-strand is shown as red spheres and interlocks with the β-bulge. Following straightening of the β-bulge, one to three water molecules (shown as blue spheres) enter the periphery of the hydrophobic cleft flanked by residues Pro^{95}, Trp^{112} and Tyr^{122} on the A-, B- and C- strands, respectively.

an extension of 4 Å. The tilt angle, defined as the angle between the N-terminal C_α (Gly^1), the middle linker's C_α (Val^{91}), and the C-terminal C_α (Thr^{184}), increases initially from 140° to approximately 175°. Consequently, an additional 6 Å results from the straightening of this angle along the force vector. The remaining 3 Å extension results from changes within the modules. In this pre-stretched state, the modules remain in their twisted state as defined in our earlier work (Craig et al., 2001). That is, the upper and lower β-sheets remain twisted approximately 30° relative to each other (Fig. 3a,b).

We monitored the time-dependent changes in the spatial orientation between the synergy site and RDG-loop, as it has been suggested that their relative orientation towards one another plays a critical role in their adhesiveness to integrin $\alpha_5\beta_1$ (Garcia et al., 1999; Grant et al., 1997; Hamburger et al., 1999; Redick et al., 2000). Throughout the rapid initial extension and the ensuing pre-stretched state, the orientation of the RGD-loop relative to the synergy site remained essentially the same. Fig. 2b shows the distance between the RGD-loop and the synergy site, defined as the length of the vector connecting the C_α of Arg^{54} to the C_α of Arg^{168}. This distance remained within 35 ± 2 Å despite a 20-Å increase in total extension during this period. Fig. 2c displays the rotation between the two sites, defined as the torsional dihedral angle formed by atoms C_α of Arg^{54}, the center of masses for FN-III$_9$ and FN-III$_{10}$, and C_α of Arg^{168}. This angle remained between 15° and 20° during this time frame, so that both sites were always located on the same face of the protein.

3.3. Functionally decoupled state

Extension beyond the pre-stretched state of FN-III$_{9-10}$ consistently began with a key sequence of events mainly involving FN-III$_{10}$. These events all occurred at the end of the first plateau in the extension–time plot (Fig. 2a) and were found to be consistent with earlier SMD studies on single FN-III modules. The first of these events consisted of the breaking of two backbone hydrogen bonds between Arg^{96} and Asp^{113}. This event was immediately followed by straightening of the adjacent β-bulge in the A-strand and resulted in a large enough gap between the A- and G-strands for 1–3 water molecules to penetrate and solvate the periphery of the hydrophobic core consisting of Pro^{95}, Trp^{112} and Tyr^{122} (Fig. 4). These events occurred with minimal extension (less than 3 Å) of FN-III$_9$ and FN-III$_{10}$. After this partial solvation of the periphery of its core, the FN-III$_{10}$ module continued to extend, resulting in an increase in the distance between the intact RGD-loop of FN-III$_{10}$

and the synergy site of FN-III$_9$ to 55 Å. We, therefore, refer to this intermediate state of FN-III$_{9-10}$ as the 'functionally decoupled' state. Extension in the functionally decoupled state occurred primarily within the FN-III$_{10}$ module, which extended by 23 Å (225–600 ps), whereas FN-III$_9$ extended by only 4 Å within the same time frame. Likewise, the C_α RMSD for FN-III$_{10}$ increased from 2.5 to 9.5 Å, relative to the equilibrated structure, compared to an increase from 2.1 to 2.4 Å for FN-III$_9$. Throughout this extension, the tertiary structure of both modules remained largely intact without unraveling β-strands from either module. Most of the structural changes seen in FN-III$_{10}$ during the functionally decoupled state took place in the first half of this time frame, between 225 and 425 ps, where it extended from 12 to 30 Å. During this extension, the β-strands from opposing β-sheets aligned parallel to one another, whereas in both the equilibrated and pre-stretched state the β-strands remained twisted with respect to one another by approximately 30°. These results are consistent with our previous single module studies, in which we first proposed the existence of an aligned state in the forced-unfolding trajectory. After FN-III$_{10}$ reaches the aligned state, both FN-III$_9$ and FN-III$_{10}$ extend more gradually. FN-III$_{10}$ was observed to extend from 30 to 35 Å with an RMSD increase of 6.3 to 9.5 Å. While earlier studies on single FN-III modules showed a distinct plateau in the time–extension plots during the aligned state of FN-III$_{10}$, these simulations on FN-III$_{9-10}$ describe a region of gradual extension. The gradual extension results from slipping between the upper G- and lower A-strand in FN-III$_{10}$ and from the rupture of a hydrogen bond at the C-terminus that allows the terminal peptide chain to further extend.

The relative orientations of the synergy site and the RGD-loop changed dramatically as FN-III$_{9-10}$ extended from the pre-stretched native state to the functionally decoupled state. The distance between the RGD and the synergy site increased by 20 Å to reach a plateau at 55 ± 3 Å (Fig. 2b). At the same time, the two modules rotated approximately 50° relative to each other in this simulation for an overall torsional rotation of 70° between the two sites. Both the distance and rotation fluctuated within a narrow range during the regime of the functionally decoupled state (Fig. 2b,c). The rotational movement between modules FN-III$_9$ and FN-III$_{10}$ further suggest that the orientations of the RGD-loop and synergy site are not well-defined and thus the two sites are functionally decoupled in this state.

3.4. Unraveling of the first β-strand

The breakage of several backbone hydrogen bonds connecting FN-III$_{10}$'s F- and G-strands resulted in a separation of the G-strand from the rest of the module and a breakdown of its tertiary structure. Previous simulations on single modules suggest that the A-strand may also unravel first (Craig et al., 2001). Breakage of these backbone hydrogen bonds can be correlated with the largest force peaks in cv-SMD simulations, and the beginning of a rapid extension out of the functionally decoupled state (seen at 600 ps in Fig. 2a). We observed variability in the unfolding pathway beyond this point.

3.5. Comparison to previous studies

Previous molecular dynamics simulations modeling the forced unfolding of FN-III modules have either solvated the protein in a spherical water bubble (Craig et al., 2001; Krammer et al., 1999; Lu et al., 1998; Lu and Schulten, 2000) or used an implicit solvent model (Paci and Karplus, 1999, 2000) rather than using a periodic box simulation as described here. It is of interest to determine how the observations described here compare to earlier simulations on FN-III modules. The simulations of Paci et al. showed FN-III$_9$ unfolding prior to FN-III$_{10}$, whereas our results indicate that unraveling consistently began with the FN-III$_{10}$ module or concomitantly in both modules. A more detailed comparison of these two models as they relate to mechanical stability is provided elsewhere (Craig et al., 2001; Paci and Karplus, 1999).

The results presented here are consistent with our earlier studies on single FN-III modules solvated by a spherical water bubble. Those same studies showed that FN-III modules extend from a twisted state into an aligned state before the FN-III tertiary structure unravels. In addition, those results revealed that the energy barrier separating the twisted and aligned states is significantly smaller for FN-III$_{10}$ than for FN-III$_9$. Therefore, it is not surprising that in the simulations presented here, the transition from the twisted to aligned state of FN-III$_{10}$ occurs first and results in the extension from the pre-stretched to the functionally decoupled state. Hence, the pre-stretched state for FN-III$_{9-10}$ is characterized by having both FN-III$_9$ and FN-III$_{10}$ in the twisted state, while the functionally decoupled state is characterized by FN-III$_9$ remaining in a twisted state but FN-III$_{10}$ being extended into the aligned state (Craig et al., 2001).

4. Discussion

Our simulations of the forced unfolding pathway of FN-III$_{9-10}$ indicate that two characteristic states exist prior to the force-induced separation of the first β-strand of FN-III$_{10}$. First, the pre-stretched state was reached following the straightening of the terminal ends and a reduction of the tilt angle between the adjacent modules. Despite a 30% extension from the equilibrated state, the relative orientation of the RGD-loop and the synergy

site in the pre-stretched state remain similar to the equilibrated structure: the distance between the synergy site and the RGD-loop was approximately 35 Å with a torsional rotation of 15–20° with respect to each other. Second, the functionally decoupled state resulted from structural changes in FN-III$_{10}$ as it transitioned from a twisted to an aligned β-sheet conformation, as described in previous studies (Craig et al., 2001). These changes resulted in an increase in the RGD-synergy distance from 35 to 55 Å, as well as an increase in the rotation angle between the two modules such that the RGD-loop and synergy sites were no longer on the same face. This change in distance and relative orientation of the synergy site and the RGD-loop leads to a decoupling of their biological functions. Upon unraveling of the FN-III$_{10}$ module, the RGD-loop straightened, thus yielding it inaccessible to RGD mediated integrin binding. When considered in the light of previous independent experimental reports, these structural predictions on stretch-induced conformational changes have significant functional implications regarding FN-integrin interactions and downstream cell signaling events.

Several experimental observations suggest that a 35-Å separation of the RGD-loop and synergy site, found in the native and pre-stretched states, is optimal for binding the $\alpha_5\beta_1$ integrin. In particular, splicing two amino acids in the linker chain separating FN-III$_9$ and FN-III$_{10}$ reduces the efficiency of the FN-III$_{9-10}$ in mediating or competitively inhibiting spreading of $\alpha_5\beta_1$-expressing cells by 5–10-fold (Grant et al., 1997). For comparison, two residues in an extended peptide chain would add approximately 7 Å to the overall extension. In the same report, the addition of six amino acids (the equivalent of 21 Å) essentially eliminated the ability of the FN-III$_{9-10}$ pair to mediate or inhibit spreading, reducing it to the same activity as observed for the FN-III$_{10}$ module alone. Thus, the distance increase from 35 to 55 Å observed by SMD in the functionally decoupled state is predicted to essentially eliminate the effect of the synergy site on $\alpha_5\beta_1$ binding. Additional evidence that a 35 Å separation leads to optimal binding is provided by the bacterial adhesion protein, invasin. Invasin binds integrin $\alpha_5\beta_1$ 25–100 times more strongly than does FN, and has a rigid structure lacking a flexible hinge region within the integrin-binding site (Hamburger et al., 1999), suggesting that invasin is structurally comparable to the integrin-bound conformation of FN. The two regions that are critical for integrin binding and are homologous to the RGD-loop and synergy site (Leong et al., 1995; Saltman et al., 1996) are separated by 32 Å in the crystal structure (Hamburger et al., 1999). In addition, the integrin α_5-subunit has been shown to be capable of binding both FN-III$_9$ and FN-III$_{10}$ (Baneres et al., 1998), and α-subunits consist of a β-propeller structure that is only 35 Å wide (Xiong et al., 2001).

Our simulations thus suggest that mechanical tension can have three possible effects on FN-III$_{9-10}$ binding to integrins. First under low tension, FN-III$_{9-10}$ would only stretch to the pre-stretched state where the RGD-synergy site distance is optimal to bind the $\alpha_5\beta_1$ integrin, and structurally close to the equilibrated structure. Second, under moderate tension, FN-III$_{9-10}$ would stretch to the functionally decoupled state and exhibit greatly reduced $\alpha_5\beta_1$ binding as described above. Because the RGD-loop is intact in this state, integrins such as $\alpha_v\beta_3$ that do not recognize the synergy site (Bowditch et al., 1994) would bind with affinities similar to the equilibrated state. Although the binding affinity of $\alpha_5\beta_1$ would decrease at this tension, binding to $\alpha_v\beta_3$ would be unaffected. Third, under high tension, the RGD-loop would be straightened or highly distorted, eliminating RGD binding to integrins such as $\alpha_5\beta_1$ and $\alpha_v\beta_3$ (Krammer et al., 1999). While the nanosecond time window provided by SMD is not capable to predict the absolute forces at which these structural transitions occur under physiological conditions, SMD is well suited to formulate hypotheses regarding the sequence of events and how stretching might alter the structure and thus function of FN-III$_{9-10}$. This notion that the sequence of key events is not critically dependent on the force or velocity by which the system is pulled apart is supported by experimental findings on ligand–receptor dissociation. The dissociation of two model ligands from their receptors involved the passage through one or more intermediate states prior to complete dissociation. While the height of the respective activation barriers decreased with the external force and the detachment force increased with the loading rate (force/time), the sequence of events was independent of the applied force or loading rate (Evans, 1999).

The major new structural prediction of our SMD simulations is the existence of a functionally decoupled state with reduced $\alpha_5\beta_1$ binding, while other integrins that do not recognize the synergy site would bind with equal strength to the native and the functionally decoupled state of FN-III$_{9-10}$. The possibility that mechanical stretching of FN can differentially regulate the binding of FN to different members of the integrin family has profound implications in cell signaling. Different extracellular matrix proteins bind different sets of integrins, thereby activating different combinations of mitogen-activated protein (MAP) kinase signaling pathways (Giancotti and Ruoslahti, 1999). FN-mediated cell adhesion, for example, leads to a potent activation of the extracellular regulated kinases (ERKs) 1 and 2 (Danen and Yamada, 2001). Once activated, ERK translocates to the nucleus and regulates gene expression, thereby modifying other cytoplasmic substrates. Different kinase pathways can regulate cellular functions antagonistically. For example, $\alpha_5\beta_1$ binding to FN was shown to activate calcium-calmodulin dependent kinase II in K562 cells,

while binding of transfected $\alpha_v\beta_3$ to FN inhibited this kinase in these same cells (Blystone et al., 1999). Similarly, clustering of $\alpha_5\beta_1$ in smooth muscle cells was shown to activate calcium channels, while ligation and clustering of $\alpha_v\beta_3$ cells inhibited these calcium channels (Wu et al., 1998). Furthermore, some surface-adsorbed conformations of FN-III_{9-10} preferentially bind $\alpha_v\beta_3$ over $\alpha_5\beta_1$ and induce cell proliferation, while other surface-absorbed conformations preferentially bind $\alpha_5\beta_1$ over $\alpha_v\beta_3$ and induce cell differentiation (Garcia et al., 1999). While the particular effect on a cell may prove to depend on how the integrin signaling network connects to downstream effects, our results provide a structural mechanism through which a FN matrix may have opposite effects on a cell depending on whether it is relaxed or under moderate tension. Indeed, certain integrins are vital for cell responses to mechanical stimuli [reviewed in Shyy and Chien (1997)]. In addition, the shape of the cell's cytoskeleton and extracellular matrix, as well as the forces they experience, are as important in determining cell fate as are the proteins within the matrix (Chen et al., 1997) [for review, see Chicurel et al., (1998)]. Taken together, these simulations provide a structural model that describes how mechanical stimuli could regulate differential integrin binding, thus translating a mechanical into a chemical signal.

Our simulations predict how tension on FN affects the affinity of integrins for FN binding sites that are not occupied. They do not, however, predict what will happen to integrins that are already bound. Though integrins are localized in focal adhesions where they connect FN fibrils to the cell cytoskeleton, and are, therefore, likely to be a source of tension to FN, simulating the effect of force after integrin binding is beyond the scope of this paper. Nevertheless, the sequence of unfolding events in our simulations poses the question of whether it is by accident or design that FN contains symmetric disulfide cross-linked dimers with the FN-III_{9-10} modules oriented with the synergy site away and RGD-loop towards the center of the FN dimer (see Fig. 1). These dimers are assembled into fibrils whose terminal ends are anchored in cell adhesion sites such that cells can stretch the fibers (Pankov et al., 2000). Each FN-III_{9-10} subunit within the fiber will experience isometric forces from both of its termini. At the end of a FN fiber, however, the last integrin-bound FN-III_{9-10} subunit experiences forces only through one end by its connection to the fiber, namely the C-terminus. The tension from the fiber is balanced by FN-III_{10}'s RGD-mediated anchorage to an integrin, while FN-III_{10}'s N-terminus and the adjacent FN-III_9 are not under tension. The lack of tension on the N-terminus of FN-III_{10} implies that the distance of the RGD-loop to synergy site on this terminal FN-III_9 would be unaffected by tension, even under conditions where the other FN-III_{9-10} subunits within the fiber are stretched into the functionally decoupled state. Thus, the orientation of FN-III_{9-10} and FN in fibrils provides a mechanism that would allow $\alpha_5\beta_1$ integrins at the ends of fibrils, but not those along their lengths, to bind under high tensions. This hypothesis provides an explanation for why fine FN fibrils co-localize with $\alpha_5\beta_1$ integrins primarily at the ends of their fibers as well as at cell-FN contacts under high tension (Christopher et al., 1997; Wennerberg et al., 1996; Zamir et al., 1999, 2000).

In summary, SMD gives the first structural insights into how mechanical stretching of FN may alter the structure and thus the function of the cell-binding module FN-III_{9-10}. The existence of the functionally decoupled state has the advantage that the synergistic effect can be turned off mechanically by inflicting a small structural perturbation that occurs prior to unraveling the modules. Since FN's fibrillar networks couple cells mechanically to their environment and to neighboring cells, it is important to learn how mechanical forces may regulate the exposure and relative distances of FN's binding sites and potentially control outside-in cell signaling.

Acknowledgments

We would like to thank Dr Gretchen Baneyx, Loren Baugh, Meher Antia, John Saeger, and Dr T.P. Lybrand for their many contributions and fruitful discussions. The research was supported by a NIH grant (R01 GM49063; VV), NCRR Resource for Biomolecular Modeling (NIH PHS 5 P41 RR05969; KS), a NIH molecular biophysics training grant fellowship (NIH 5 T32 GM08268, DC), a NSF computer time grant (MCA93S028; KS), and a Whitaker Foundation Graduate Fellowship (WT).

References

Baneres, J.L., Roquet, F., Green, M., LeCalvez, H., Parello, J., 1998. The cation-binding domain from the alpha subunit of integrin $\alpha_5\beta_1$ is a minimal domain for fibronectin recognition. J. Biol. Chem. 273, 24744–24753.

Blystone, S.D., Slater, S.E., Williams, M.P., Crow, M.T., Brown, E.J., 1999. A molecular mechanism of integrin crosstalk: $\alpha_v\beta_3$ suppression of calcium/calmodulin-dependent protein kinase II regulates alpha5beta1 function. J. Cell Biol. 145, 889–897.

Bowditch, R.D., Hariharan, M., Tominna, E.F., et al., 1994. Identification of a novel integrin binding site in fibronectin. Differential utilization by β_3 integrins. J. Biol. Chem. 269, 10856–10863.

Chen, C.S., Mrksich, M., Huang, S., Whitesides, G.M., Ingber, D.E., 1997. Geometric control of cell life and death. Science 276, 1425–1428.

Chicurel, M.E., Chen, C.S., Ingber, D.E., 1998. Cellular control lies in the balance of forces. Curr. Opin. Cell Biol. 10, 232–239.

Christopher, R.A., Kowalczyk, A.P., McKeown-Longo, P.J., 1997. Localization of fibronectin matrix assembly sites on fibroblasts and endothelial cells. J. Cell Sci. 110, 569–581.

Corbett, S.A., Schwarzbauer, J.E., 1999. Requirements for $\alpha_5\beta_1$ integrin-mediated retraction of fibronectin-fibrin matrices. J. Biol. Chem. 274, 20943–20948.

Craig, D., Krammer, A., Schulten, K., Vogel, V., 2001. Comparison of the early stages of forced unfolding for fibronectin type III modules. Proc. Natl. Acad. Sci. USA 98, 5590–5595.

Danen, E.H., Aota, S., van Kraats, A.A., Yamada, K.M., Ruiter, D.J., van Muijen, G.N., 1995. Requirement for the synergy site for cell adhesion to fibronectin depends on the activation state of integrin $\alpha_5\beta_1$. J. Biol. Chem. 270, 21612–21618.

Danen, E.H., Yamada, K.M., 2001. Fibronectin, integrins, and growth control. J. Cell Physiol. 189, 1–13.

Evans, E., 1999. Looking inside molecular bonds at biological interfaces with dynamic force spectroscopy. Biophys. Chem. 82, 83–97.

Garcia, A.J., Vega, M.D., Boettiger, D., 1999. Modulation of cell proliferation and differentiation through substrate-dependent changes in fibronectin conformation. Mol. Biol. Cell 10, 785–798.

Giancotti, F.G., Ruoslahti, E., 1999. Integrin signaling. Science 285, 1028–1032.

Grant, R.P., Spitzfaden, C., Altroff, H., Campbell, I.D., Mardon, H.J., 1997. Structural requirements for biological activity of the ninth and tenth FIII domains of human fibronectin. J. Biol. Chem. 272, 6159–6166.

Hamburger, Z.A., Brown, M.S., Isberg, R.R., Bjorkman, P.J., 1999. Crystal structure of invasin: a bacterial integrin-binding protein. Science 286, 291–295.

Isralewitz, B., Baudry, J., Gullingsrud, J., Kosztin, D., Schulten, K., 2001. Steered molecular dynamics investigations of protein function. J. Mol. Graph Model 19, 13–25.

Isralewitz, B., Gao, M., Schulten, K., 2001. Steered molecular dynamics and mechanical functions of proteins. Curr. Opin. Struct. Biol. 11, 224–230.

Jorgensen, W.L., Chandrasekhar, J., Madura, J.D., Impey, R.W., Klein, M.L., 1983. Comparison of simple potential functions for simulating water. J. Chem. Phys 79, 926–935.

Kale, L., Robert, S.M.B., Brunner, R., et al., 1999. NAMD2: Greater scalability for parallel molecular dynamics. J. Comput. Phys. 151, 283–312.

Kellermayer, M.S.Z., Smith, S.B., Granzier, H.L., Bustamante, C., 1997. Folding–unfolding transitions in single titin molecules characterized with laser tweezers. Science 276, 1112–1116.

Krammer, A., Lu, H., Isralewitz, B., Schulten, K., Vogel, V., 1999. Forced unfolding of the fibronectin type III module reveals a tensile molecular recognition switch. Proc. Natl. Acad. Sci. USA 96, 1351–1356.

Leahy, D.J., Aukhil, I., Erickson, H.P., 1996. 2.0 Å crystal structure of a four-domain segment of human fibronectin encompassing the RGD loop and synergy region. Cell 84, 155–164.

Leong, J.M., Morrissey, P.E., Marra, A., Isberg, R.R., 1995. An aspartate residue of the *Yersinia pseudotuberculosis* invasin protein that is critical for integrin binding. EMBO J. 14, 422–431.

Lu, H., Isralewitz, B., Krammer, A., Vogel, V., Schulten, K., 1998. Unfolding of titin immunoglobulin domains by steered molecular dynamics simulation. Biophys. J. 75, 662–671.

Lu, H., Schulten, K., 1999. Steered molecular dynamics simulation of conformational changes of immunoglobulin domain I27 interpret atomic force microscopy observations. Chem. Phys. 247, 141–153.

Lu, H., Schulten, K., 2000. The key event in force-induced unfolding of titin's immunoglobulin domains. Biophys. J. 79, 51–65.

MacKerell, A.D., Bashford, D., Bellot, M., et al., 1998. All-hydrogen empircal potential for molecular modeling and dynamics studies of proteins using the CHARMM22 force field. J. Phys. Chem. B 102, 3586–3616.

Marszalek, P.E., Lu, H., Li, H., et al., 1999. Mechanical unfolding intermediates in titin modules. Nature 402, 100–103.

Oberdorfer, Y., Fuchs, H., Janshoff, A., 2000. Conformational analysis of native fibronectin by means of force spectroscopy. Langmuir 16, 9955–9958.

Oberhauser, A.F., Marszalek, P.E., Erickson, H.P., Fernandez, J.M., 1998. The molecular elasticity of the extracellular matrix protein tenascin. Nature 393, 181–185.

Paci, E., Karplus, M., 1999. Forced unfolding of fibronectin type 3 modules: an analysis by biased molecular dynamics simulations. J. Mol. Biol. 288, 441–459.

Paci, E., Karplus, M., 2000. Unfolding proteins by external forces and temperature: the importance of topology and energetics. Proc. Natl. Acad. Sci. USA 97, 6521–6526.

Pankov, R., Cukierman, E., Katz, B.Z., et al., 2000. Integrin dynamics and matrix assembly: tensin-dependent translocation of $\alpha_5\beta_1$ integrins promotes early fibronectin fibrillogenesis. J. Cell Biol. 148, 1075–1090.

Redick, S.D., Settles, D.L., Briscoe, G., Erickson, H.P., 2000. Defining fibronectin's cell adhesion synergy site by site-directed mutagenesis. J. Cell Biol. 149, 521–527.

Rief, M., Gautel, M., Oesterhelt, F., Fernandez, J.M., Gaub, H.E., 1997. Reversible unfolding of individual titin immunoglobulin domains by AFM. Science 276, 1109–1112.

Saltman, L.H., Lu, Y., Zaharias, E.M., Isberg, R.R., 1996. A region of the *Yersinia pseudotuberculosis* invasin protein that contributes to high affinity binding to integrin receptors. J. Biol. Chem. 271, 23438–23444.

Sechler, J.L., Corbett, S.A., Schwarzbauer, J.E., 1997. Modulatory roles for integrin activation and the synergy site of fibronectin during matrix assembly. Mol. Biol. Cell. 8, 2563–2573.

Shyy, J.Y., Chien, S., 1997. Role of integrins in cellular responses to mechanical stress and adhesion. Curr. Opin. Cell Biol. 9, 707–713.

Wennerberg, K., Lohikangas, L., Gullberg, D., Pfaff, M., Johansson, S., Fassler, R., 1996. β_1 integrin-dependent and -independent polymerization of fibronectin. J. Cell Biol. 132, 227–238.

Wu, X., Mogford, J.E., Platts, S.H., Davis, G.E., Meininger, G.A., Davis, M.J., 1998. Modulation of calcium current in arteriolar smooth muscle by $\alpha_v\beta_3$ and $\alpha_5\beta_1$ integrin ligands. J. Cell Biol. 143, 241–252.

Xiong, J.P., Stehle, T., Diefenbach, B., et al., 2001. Crystal structure of the extracellular segment of integrin $\alpha_v\beta_3$. Science 294, 339–345.

Zamir, E., Katz, B.Z., Aota, S., Yamada, K.M., Geiger, B., Kam, Z., 1999. Molecular diversity of cell-matrix adhesions. J. Cell Sci. 112, 1655–1669.

Zamir, E., Katz, M., Posen, Y., et al., 2000. Dynamics and segregation of cell-matrix adhesions in cultured fibroblasts. Nat. Cell Biol. 2, 191–196.